Fibrin protofibril packing and clot stability are enhanced by extended knob-hole interactions and catch-slip bonds

Nathan L. Asquith[1,2], Cédric Duval[1], Artem Zhmurov[3,4,5], Stephen R. Baker[1], Helen R. McPherson[1], Marco M Domingues[1,6], Simon D. A. Connell[7], Valeri Barsegov[8], Robert A. S. Ariëns[1]

[1] Discovery and Translational Science Department, Leeds Institute of Cardiovascular And Metabolic Medicine, School of Medicine, University of Leeds, UK

[2] Vascular Biology Program, Karp Research Laboratories, 1 Blackfan Circle, Boston Children's Hospital; Harvard Medical School, Boston, MA, USA 02215

[3] The EuroCC National Competence Center Sweden, 114 28 Stockholm, Sweden

[4] PDC Center for High Performance Computing, KTH Royal Institute of Technology, 100 44 Stockholm, Sweden

[5] Science for Life Laboratory, Box 1031, 171 21 Solna, Sweden

[6] Institute of Molecular Medicine, Faculty of Medicine, University of Lisbon, Portugal

[7] Molecular and Nanoscale Physics Group, School of Physics and Astronomy, University of Leeds, UK

[8] *Department of Chemistry, University of Massachusetts, Lowell, MA, USA*

SUPPLEMENTARY ONLINE MATERIAL

Supplementary Methods

Materials: Human thrombin (Merck; Feltham, UK) was reconstituted to 250U/ml and stored in aliquots at -80°C. All other chemicals were obtained from Sigma-Aldrich (Gillingham, UK) unless stated otherwise. Tris-buffered saline (TBS, 50mM Tris-Base, 100mM NaCl, pH 7.4) was used unless otherwise stated. Reptilase (Stago, Diagnostics; Reading, UK) was used at a final concentration of 0.5BU/mL, human tPA (Pathway Diagnostics; Dorking, UK) was used at a final concentration of 6nM, human plasminogen (Enzyme Research laboratories) was used at a final concentration of 0.4μM.

SDS-PAGE: Samples were prepared using 2.5μg protein, 1xNuPage LDS sample buffer, 1xNuPAGE sample reducing agent (ThermoFisher-Scientific; Loughborough, UK) and TBS. Samples were incubated at 70°C for 10min and loaded onto NuPage 4-12% Bis-Tris Gels (ThermoFisher-Scientific) alongside Precision Plus Protein molecular weight ladder (Bio-Rad; Hempstead, UK). Gels were run in NuPAGE MES SDS running buffer at 200V for 90min, stained with Gel Code® Blue Stain reagent (ThermoFisher-Scientific), de-stained using de-ionised H_2O and imaged using Gbox imaging system (Syngene; Cambridge, UK).

Recombinant fibrinogen expression: Highly expressing clones were selected by using L-histidinol and the expression levels were determined by an in-house fibrinogen ELISA. Recombinant WT and all fibrinogen variants were expressed in roller bottles coated with cytodex microcarrier beads using DMEM-F12 (Thermo-Fisher Scientific; Loughborough, UK) supplemented with 4μg/mL aprotinin and ITS supplement (Insulin, 5μg/mL, transferrin 5μg/mL, sodium selenite 5ng/mL. Roche; Welwyn Garden City, UK). Expressed fibrinogen was secreted into the medium and harvested every 48hr for 8 weeks. PMSF 150mM was added to the harvested medium before storing at -40°C. The harvested medium was defrosted and precipitated overnight at 4°C with 40% ammonium sulphate (VWR International; Lutterworth UK) and a protease inhibitor mix (5mM ε-aminocaproic acid (ε-ACA), 5mM benzamidine, 1μM pepstatin, 1μM Leupeptin, 100mM PMSF, and 20mM 2-(N-morpholino) ethanesulfonic acid (pH 5.6)). The precipitate was centrifuged at 14,500g for 45min without brakes at 4°C in an Avanti J-265 XPI (Beckman Coulter; California USA). The pellet was resuspended and incubated at 4°C with a second protease inhibitor mix (5mM ε-ACA, 5mM benzamidine, 5μM Pepstatin, 5μM Leupeptin,100mM PMSF, 10U/mL Soybean trypsin inhibitor, 1mM EDTA, 300mM NaCl, 200mM Tris, pH 7.4) and centrifuged at 43,000g for 30min. Supernatants were purified by immunoaffinity chromatography (IF-1 mAb, 10mg. Kamiya Biomedical; Seattle USA) using an ÄKTA Avant 25 (GE Healthcare; Little Chalfont, UK) as previously described[1]. The fibrinogen fractions were pooled, concentrated and dialysed into TBS and stored at -80°C. Protein integrity was determined by SDS-PAGE.

Experiment-specific clotting conditions: Note that different clotting conditions were used for each assay used to interrogate the role(s) of the extended knob-hole interactions. Concentrations were chosen allow for the most detailed scientific comparison for each

assay, specifically ensuring that the assays are performed within their respective window of optimal sensitivity and specificity. Although experimental conditions vary, in each experiment the test samples are compared to its relative WT control, providing like-for-like comparisons. For each method description, we specify the optimal experimental conditions below.

Confocal Microscopy: Sample preparation and LSCM imaging parameters were adapted from previous work [1]. Fibrinogen variants were labelled using the Alexa Fluor 488 protein labelling kit (Thermo-Fisher Scientific) following the manufacturer's instructions. Clots were formed by the combination of 0.475mg/mL non-labelled fibrinogen and 0.025mg/mL AlexaFluor 488 labelled fibrinogen with a reaction mix containing 5mM $CaCl_2$ and 0.1U/mL thrombin (final concentrations) in TBS with a total volume of 40µl. Next, 3 µl was transferred to a channel in a VI flow, uncoated sterile µ-slide (Ibidi GmbH; Gräfelfing, Germany), placed into a dark humidity chamber and allowed to clot for 1hr. Micrographs of a z-stack (15µm, 21 slices) of the final clot structure were taken with an 880 LSCM with a 40x 1.4 DIC M27 oil immersion objective (Zeiss; Cambridge, UK). Three z-stacks were imaged at a minimum. The software package ZEN (Zeiss) was used to flatten the z-stacks into a 2D image. Using ImageJ software (National Institutes of Health; Bethesda, MD, USA), three lines spanning the entire length of the micrograph were drawn horizontally and vertically, and the number of fibers that intersected these lines were counted and used as a reflection of clot density.

Confocal Microscopy (Lysis): The samples prepared for density experiments were subsequently lysed by the addition of 6nM tPA and 0.4µM of human plasminogen. The configuration of the chamber allowed the addition of this lysis cocktail to be concentrated at one side of the clot allowing the real-time imaging of a lysis front. The rate of lysis was then calculated by the time taken for the lysis front to travel a set distance of the chamber, using ImageJ.

Scanning electron Microscopy: Scanning electron microscopy sample preparation and imaging was adapted from previous work[2]. Fibrin clots were made to the final concentration of 0.5mg/mL fibrinogen, 10mM $CaCl_2$ and 1U/mL thrombin, in TBS buffer with a total volume of 80µl, and immediately transferred to a pierced Eppendorf lid reaction chamber sealed at the bottom with parafilm. Clots were allowed to form in a humidity chamber for hr, the parafilm was removed and clots were washed 3 times in 50mM sodium cacodylate buffer (pH 7.4) for 20min. Clots were fixed with 2% Gluteraldehyde for a period of 2hr, washed another three times in 50mM sodium cacodylate buffer (pH 7.4) and dehydrated using an acetone dehydration series (30-90% and 3x 100% acetone), 15min per concentration. The clots were transferred to fresh 100% acetone before undergoing critical point drying (performed by Martin Fuller, Astbury Centre for Structural and Molecular Biology, University of Leeds, UK). Critical point dried samples were mounted onto 13mm diameter aluminium SEM imaging stubs and coated with 0.5nm layer of iridium using an Agar High resolution sputter coater (Agar Scientific; Stanstead, UK). Each clot type was made in triplicate and each individual clot was imaged at a minimum of two locations at x2,000; x5000; x10,000; x 20,000; and x50,000 magnifications using SU8230 scanning electron microscope (Hitachi; London UK). Images at x20,000 were used to calculate average fiber diameters. The images were imported into ImageJ software, a 9 x 6 line grid overlay was superimposed onto the

image, creating 54 intersections across the image, and the fibers that were closest to those intersections were measured for fiber thickness.

Atomic Force Microscopy: All reagents were filtered with a 0.22µm filter. A mica disc was cleaved and treated with 50µl of 5mM $NiCl_2$ to positively charge the surface. Fibrin clots were made with 0.02mg/mL fibrinogen, 0.05U/mL thrombin and 2mM $CaCl_2$ (final concentrations) in a total volume of 45µl. All samples were mixed gently and allowed to clot for 10 or 20min, before stopping the reaction with 135µl of TBS, and immediately transferred to the treated mica disc for 10sec. The surface was then washed with 15 µl of de-ionised H_2O and dried with nitrogen gas. Samples were imaged in quintuplicate 4x4µm windows using a Nanoscope V MultiMode 8 (Bruker; Coventry, UK) in soft tapping mode in air with Tespa-V2 tips (Bruker). Images were flattened by the third order, and streaks were removed during processing using Nanoscope Analysis v1.5 (Bruker). The modified file was exported to ImageJ for accurate analysis of protofibril lengths using the ImageJ measuring tool[3].

Microrheology of fibrin clots: Clots (0.5mg/mL fibrinogen, 5mM $CaCl_2$, 1:250 (v:v) superparamagnetic beads [Dynabeads, M-450 Epoxy. ThermoFisher-Scientific] and 0.1U/mL thrombin in TBS buffer) were formed in a microcell (50mm length, 0.5mm diameter. VitroCom; Mountain Lakes, NJ, US), before the ends of the capillary were blocked with petroleum jelly to prevent dehydration. Each clot was manually rolled for 15min to prevent bead sedimentation, after which the clot was allowed to fully form overnight at room temperature in a humidity chamber. Force measurements at 40pN were conducted for 10min per bead, to generate the time-dependent bead displacement, which was converted to the time dependent compliance. The frequency dependent storage modulus (G') and loss modulus (G") were determined from the time dependent compliance as previously demonstrated[4]. The loss tangent (tanδ) which is the ratio G"/G' was calculated to determine the overall mechanical properties of the fibrin clot at 0.1Hz, 1.0Hz and 10Hz. The displacement of 10 superparamagnetic beads were analysed per sample.

Statistical analysis: Results were analysed in GraphPad Prism 7 using One-Way ANOVA with Dunnett's multiple comparisons. All assays were conducted at least in triplicate. The outputs from pulling simulations, e.g. structures (coordinate files) and forces (energy files), were post-processed. The bond rupture force, i.e. force at which the number of residue-residue contacts stabilizing the A:a knob-hole bond *Q* is equal to zero, was extracted and averaged over 5 independent runs of dynamic force-ramp simulations.

Supplementary Results

Structure analysis of A:a knob-hole bond rupture transitions from MD simulations

We analysed tension-induced structure alterations at the A:a knob-hole binding interface observed in MD pulling simulations for the WT, single-point mutants γD297N, γK356Q, γE323Q, and triple mutant γDEK. The results showed the following: i) For γD297N, the removal of one negative charge in the movable flap in hole 'a' has a negative impact on the

binding affinity and catch bond formation. There are two positive residues and one polar residue in extended knob 'A', αArg23, αHis24 and αGln25, which can form strong electrostatic contacts with the movable flap. When the flap rotates towards the ligand, these interactions facilitate the interface closure and catch bond formation. The removal negative charge weakens these interactions to the extent that the high affinity catch bond does not form. In addition, lack of negative charge in the movable flap allows it to form stronger persistent contacts with B-domain in the γ-nodule, e.g. with residue Asp285. These interactions keep the movable flap far away from the ligand, and the binding interface is wide open (low-affinity slip bond; low 60-90pN rupture forces; Figures 7 and S5. ii) For γK356Q, mutating γLys356 to Gln removes one positive charge in the interior region in hole 'a', which allows polar Gln to interact with the positively charged αArg23, αHis24, and αGln25 in knob 'A'. These interactions lead to a decrease in size of hole 'a', interface closure, and tighter binding (high-affinity catch bond; high rupture 90-120pN rupture forces; Figures 7 and S5). iii) For γE323Q, mutation of the negatively charged Glu to polar Gln shows the role of loop I in formation of the catch bond. Position γ323 in the γ-nodule is close to αArg23-αHis24-αGln25 stretch in knob 'A', with which it forms strong electrostatic interactions in WT. Hence, losing one negative charge reduces the binding strength (low-affinity slip bond; low 60-90pN rupture forces; Figures 7 and S5). iv) For triple mutant γDEK, the effects of mutations γD297N and γE323Q overweigh the effect of mutation γK356Q. As a result, the binding interface is wide open, and the high-affinity catch bond does not form (low-affinity slip bond; low 60-90pN rupture forces; Figures 7 and S5).

References

1. Duval C, Allan P, Connell SD, Ridger VC, Philippou H, Ariens RA. Roles of fibrin alpha- and gamma-chain specific cross-linking by FXIIIa in fibrin structure and function. *Thromb Haemost*. 2014;111(5):842-850.

2. Macrae FL, Duval C, Papareddy P, et al. A fibrin biofilm covers blood clots and protects from microbial invasion. *J Clin Invest*. 2018;128(8):3356-3368.

3. Schindelin J, Arganda-Carreras I, Frise E, et al. Fiji: an open-source platform for biological-image analysis. *Nature Methods*. 2012;9:676.

4. Evans RM, Tassieri M, Auhl D, Waigh TA. Direct conversion of rheological compliance measurements into storage and loss moduli. *Phys Rev E Stat Nonlin Soft Matter Phys*. 2009;80(1 Pt 1):012501.

Supplementary Tables

Supplementary Table 1: Mutagenesis primer sequences

	Primer Sequence
D297N-R	5'-aaaaacttgtcactaggatcattgccaaaatcaaagccatcaaag-3'
D297N-F	5'-ctttgatggctttgattttggcaatgatcctagtgacaagttttt-3'
E323Q-R	5'-gcacagttgccttgaaacttatcattgtcattgtccca-3'
E323Q-F	5'-tgggacaatgacaatgataagtttcaaggcaactgtgc-3'
K356Q-R	5'-cattaggagtagatgcttgtgagtaagtgccaccttg-3'
K356Q-F	5'-caaggtggcacttactcacaagcatctactcctaatg-3'

Supplementary Figures

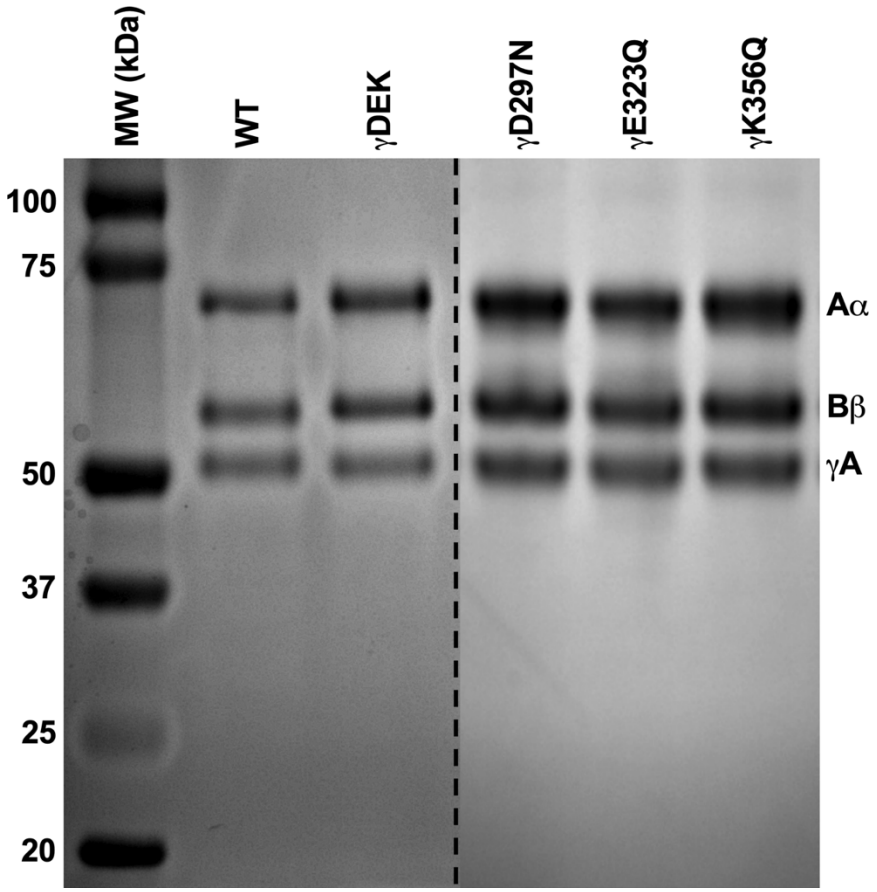

Supplementary Figure 1: Polyacrylamide gel electrophoresis of recombinant WT and variant fibrinogens. Composite image of two gels showing that the fibrinogens produced were pure and intact.

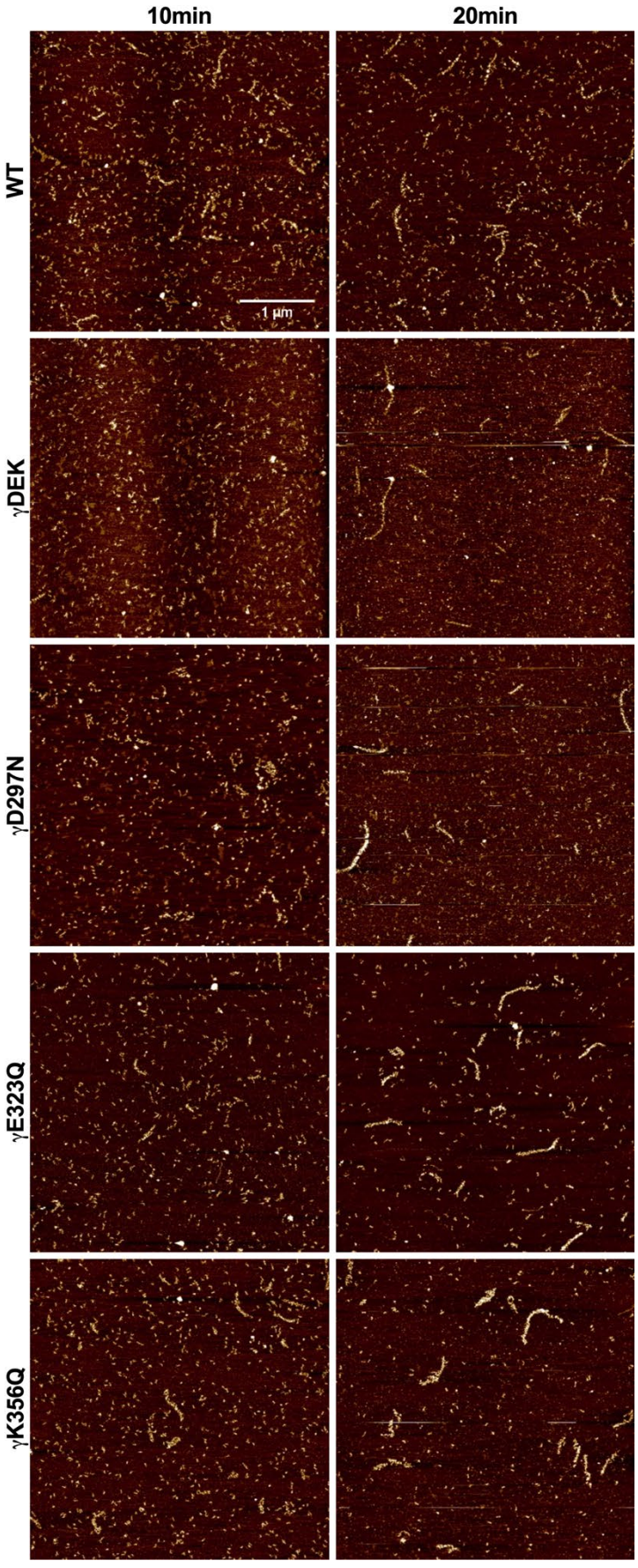

Supplementary Figure 2: Longitudinal protofibril formation. Polymerisation for WT and extended knob-hole variants was halted after 10 and 20min, prior to imaging by atomic force microscopy. Micrographs (4xµm) of the protofibrils produced for each time point showed that the protofibril length for all variants and WT increased over time. N=3.

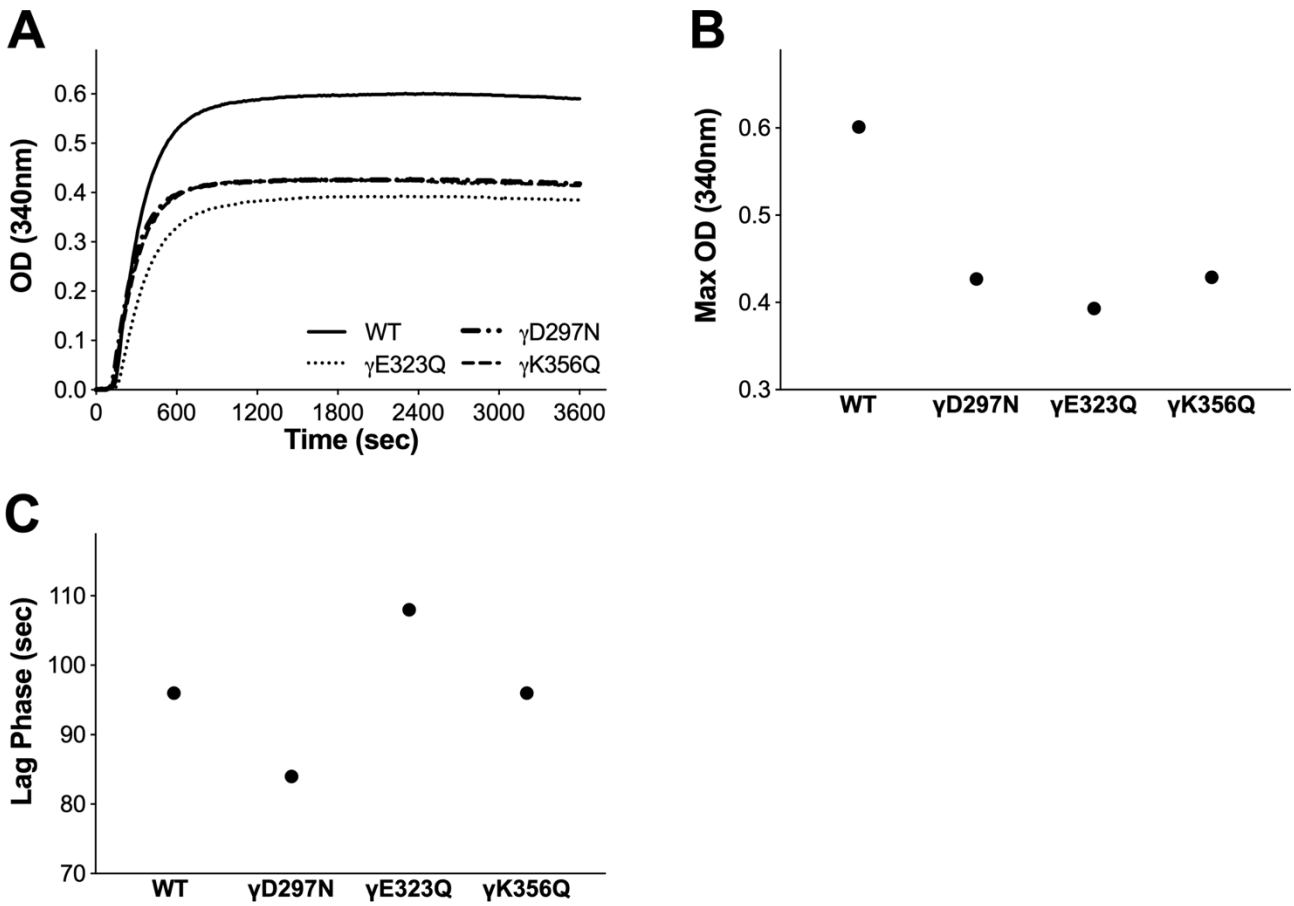

Supplementary Figure 3: Fibrin clot formation with reptilase. (A) Polymerisation profiles of WT (blue), γD297N (red), γE323Q (green), γK356Q (purple) fibrinogens using reptilase. (B) Maximum OD was reduced for all single mutant variants compared to WT. (C) Lag phase was varied for the single mutants, with γD297N being accelerated, γE323Q was extended, and γK356Q remained unchanged, compared to WT. N=1.

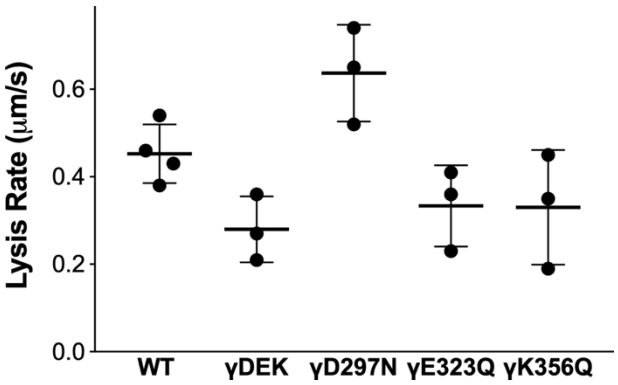

Supplementary Figure 4: Clot Lysis. Clots were formed for 1hr before lysis was induced by addition of tPA and plasminogen. The speed of the lytic front was measured, and there was no statistical significance of lysis rates compared to WT. WT N=4, variants N=3.

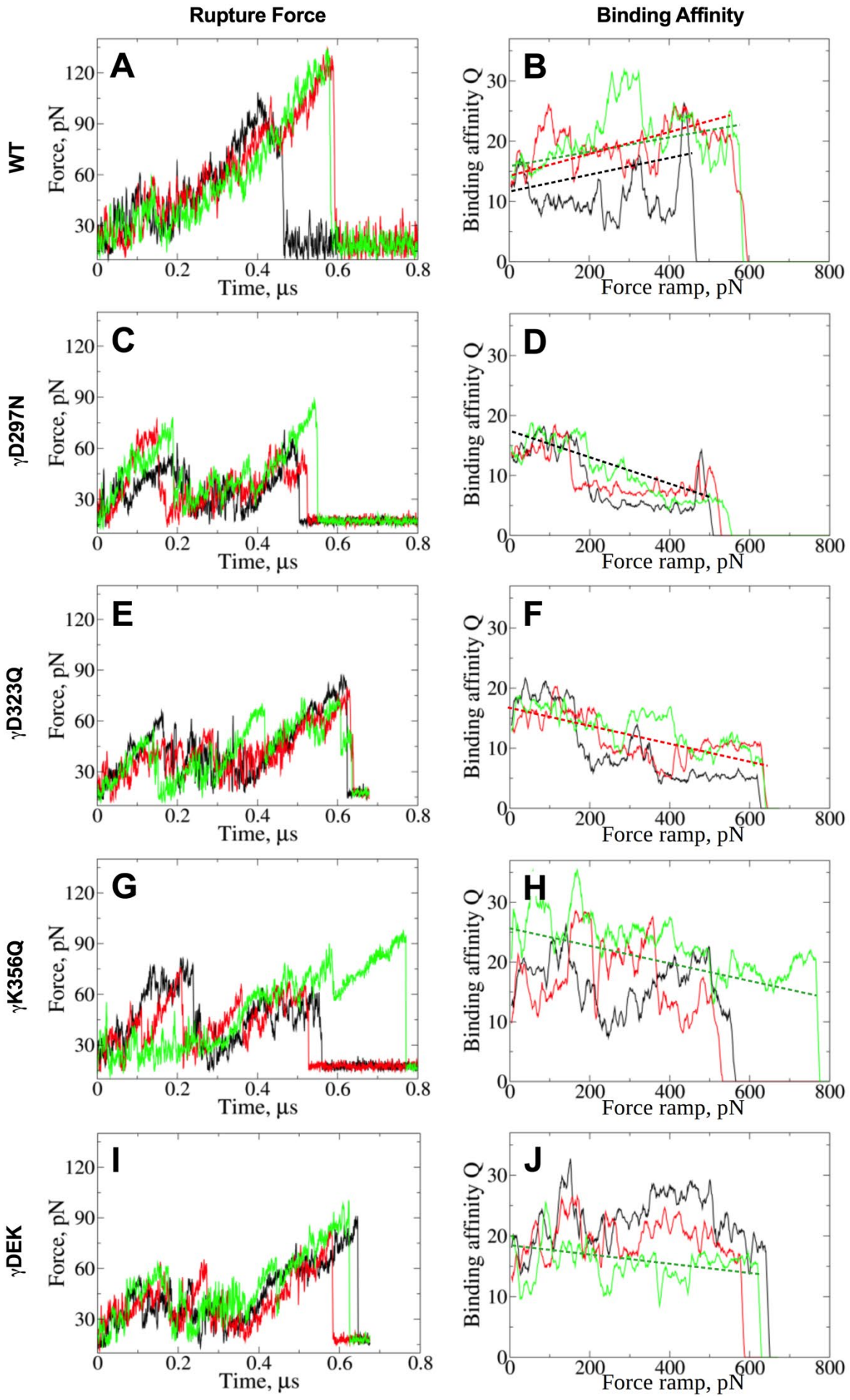
Rupture Force
Binding Affinity
WT
γD297N
γD323Q
γK356Q
γDEK
A
B
C
D
E
F
G
H
I
J
Force, pN
Time, μs
Binding affinity Q
Force ramp, pN

Supplementary Figure 5: Dynamics of A:a knob-hole bond strength. Bond rupture force vs. time (A, C, E, G, I) and binding affinity *Q* (total number of binary residue-residue contacts) vs. pulling force *f* (B, D, F, H, J). Thin dotted lines show the overall trend of the binding affinity Q as a function of the force ramp. The force maxima followed by abrupt force drops to zero (force peaks) were used to calculate the average bond-rupture forces. The force-dependence of *Q* was used to distinguish between the catch-slip type and slip type knob-hole bond rupture kinetics.